Discover Oncology

Analysis

Analysis of immune status and prognostic model incorporating lactate metabolism and immune-related genes in clear cell renal cell carcinoma

Jun Wu[1,2] · Yuqian Wu[2] · Yefeng Sun[3] · Jianhang You[4] · Wenjie Zhang[2] · Tao Zhao[5]

Received: 15 January 2025 / Accepted: 19 May 2025
Published online: 07 June 2025

Abstract

Background Clear cell renal cell carcinoma (ccRCC) is the most prevalent and highly aggressive subtype of kidney cancer. Despite the progress in research, the roles of lactate metabolism and immune-related genes (LMRGs) in its prognosis and immune microenvironment remain unclear. Until now, no studies have explored the potential impact of LMRGs on the prognosis of ccRCC and their relationship with the tumor immune microenvironment.

Methods Transcriptomic analysis was carried out using the TCGA and GEO databases. Non-negative matrix factorization (NMF) was used to subtype ccRCC samples. The Cox proportional hazards regression model and the LASSO algorithm were combined to screen the core genes related to prognosis. The Kaplan–Meier survival analysis was used to assess the relationship between these genes and patient survival. The CIBERSORT and ESTIMATE algorithms were used to analyze the level of immune infiltration.

Results Using NMF analysis, ccRCC samples were classified into two subtypes. Kaplan–Meier survival analysis revealed that patients in Cluster 2 exhibited a better prognosis than those in Cluster 1. LASSO regression analysis identified five key genes—STAT2, PDGFRL, APLNR, PRKCQ, and THRB—which were subsequently used to construct a prognostic model. The survival rate in the high-risk group was significantly lower than that in the low-risk group. Immune microenvironment analysis demonstrated that the high-risk group exhibited higher immune cell infiltration, while the low-risk group was enriched for metabolism-related pathways. Tumor mutation burden (TMB) analysis indicated that TMB synergized with the risk score. Finally, the prognostic value of these key genes was validated using the K–M database.

Conclusion Lactate metabolism and immune-related genes are of great significance in the prognostic evaluation of ccRCC. The core genes screened based on these mechanisms have the potential value as biomarkers.

Keywords Clear cell renal cell carcinoma · Lactate metabolism and immune-related genes · Prognostic signature · Tumor microenvironment

Jun Wu and Yuqian Wu have contributed equally to this work.

Supplementary Information The online version contains supplementary material available at https://doi.org/10.1007/s12672-025-02746-2.

✉ Wenjie Zhang, 71674818@qq.com; ✉ Tao Zhao, zttlwj@126.com | [1]Precision Medicine Center of Oncology, The Affiliated Hospital of Qingdao University, Qingdao 266000, China. [2]Department of Medical Oncology, People's Hospital of Rizhao, Rizhao 276826, China. [3]Department of Emergency, People's Hospital of Rizhao, Rizhao 276826, China. [4]School of Clinical Medicine, Shandong Second Medical University, Weifang 261053, China. [5]Department of Central Laboratory, Shandong Provincial Key Medical and Health Laboratory of The People's Hospital of Rizhao, Rizhao Key Laboratory of Basic Research on Anesthesia and Respiratory Intensive Care, The People's Hospital of Rizhao, Rizhao 276826, Shandong, China.

Abbreviations

ccRCC	Clear cell renal cell carcinoma
TAMs	Tumor-associated macrophages
OS	Overall survival
PFS	Progression-free survival
TME	Tumor microenvironment
DCA	Decision curve analysis
GSEA	Gene set enrichment analysis
TCIA	The cancer immunome atlas
ICIs	Immune checkpoint inhibitors
IPS	Immune therapy scores
TMB	Tumor mutational burden
NMF	Non-negative matrix factorization
PCA	Principal component analysis
Tregs	Regulatory T cells
CAMs	Cell adhesion molecules
CAF	Cancer-associated fibroblasts

1 Introduction

Clear cell renal cell carcinoma (ccRCC) is the most common type of renal tumor, accounting for 70 to 80% of all renal cancer types [1]. Although early diagnosis and surgical intervention have significantly improved the survival rate of patients [2, 3], the recurrence and metastasis of ccRCC remain a major obstacle in the clinical treatment process [4]. However, issues such as the differences in the effectiveness of individualized treatment and the inaccuracy of prognostic assessment remain the focus of our attention [5]. Therefore, searching for new biomarkers and establishing accurate prognostic models is a crucial step in the clinical management of ccRCC.

In recent years, accumulating evidence has confirmed that clear cell renal cell carcinoma (ccRCC) is fundamentally a metabolically reprogrammed tumor, characterized by enhanced glycolysis, mitochondrial dysfunction, and dysregulated lipid metabolism [6–8]. The accumulation of lactate resulting from enhanced aerobic glycolysis not only disrupts local pH homeostasis within the tumor microenvironment but also plays a crucial role in promoting immune evasion [9]. Meanwhile, previous studies have indicated that tryptophan metabolism—particularly activation of the kynurenine pathway—can influence angiogenesis and inflammatory responses in ccRCC through both immune and non-immune mechanisms, thereby shaping the immune microenvironment and promoting tumor progression [10]. Notably, ccRCC is among the most immune-infiltrated solid tumors known to date [11], and interactions between metabolic factors and immune cells such as TAMs and T cells play a pivotal role in driving immune evasion and disease progression [12]. Therefore, elucidating the coupling mechanisms between lactate metabolism and immune function may deepen our understanding of the biological nature of ccRCC and provide novel insights for prognostic stratification and therapeutic decision-making.

Given that most existing prognostic models tend to focus on a single molecule or pathway, they often fail to effectively integrate the metabolic and immune characteristics of tumors, thereby limiting their predictive performance [13]. In this study, we constructed a multidimensional prognostic model by integrating lactate metabolism-related genes (LMRGs) with immune-related differentially expressed genes, coupled with machine learning algorithms. This model not only enables more accurate prediction of patient outcomes but also reveals a potential coupling mechanism between metabolic homeostasis and immune regulation, identifying several key biomarkers with potential clinical value. These findings may provide a novel theoretical basis for the development of personalized therapeutic strategies and improve clinical management and survival benefits for patients with ccRCC.

2 Methods

2.1 Data collection sources

In this research, the ccRCC data were partitioned into a training set and a validation set. The training set data were derived from the TCGA database (https://portal.gdc.cancer.gov/), encompassing transcriptome sequencing, clinical, and mutation data of 542 tumor patients and 72 normal individuals. The validation set was obtained from the GSE167573 dataset in the GEO database (https://www.ncbi.nlm.nih.gov/geo/query/acc.cgi?acc=GSE167573), which included sequencing and survival information of patients. Immune-related genes were sourced from literature collection [14], and lactate metabolism-related genes were obtained from the MsigDB database [15] using the search keyword "Lactate."

2.2 Differential expression of LMRGs and NMF clustering analysis

The union of immune-related genes and lactate metabolism-related genes was determined through a union analysis. With the assistance of the "limma" package [16], we retrieved the expression data of immune genes and lactate metabolism genes of tumor patients and conducted data cleansing and integration to eliminate any missing portions. To compare the gene expression differences between normal and tumor patients, we set logFCfilter = 1 and fdrFilter = 0.05 as the screening criteria and presented the expression profiles of LMRGs via heatmaps and volcano plots. Based on patients' survival data, we constructed a Cox regression model and conducted nonnegative matrix factorization (NMF) analysis on prognostically relevant LMRGs ($p < 0.01$). Using the Brunet method, we clustered the selected gene expression data by testing cluster numbers ranging from 2 to 10 and determined the optimal number of clusters using the cophenetic coefficient curve. On this basis, a survival analysis of the typing results was further carried out to compare the overall survival (OS) and progression-free survival (PFS) of different types. To explore the association between typing and the tumor microenvironment (TME), the "estimate" package was utilized to score different typing samples and display them in violin plots [17]. The "MCPcounter" package was employed to analyze the immune cell infiltration status of ccRCC patients [18]. Boxplots and heatmaps illustrated the distribution differences and significance of immune cell infiltration levels among different types, and the heatmap also incorporated the TME score among different types.

2.3 Construction and validation of the prognostic model

To construct a ccRCC prognostic model based on LMRGs, TCGA samples were randomly divided into a training set (70%) and a testing set (30%). In the training set, candidate genes significantly associated with survival ($p < 0.05$) were identified using univariate Cox regression, and key genes with independent prognostic value were further selected via LASSO regression. A multivariate Cox regression model was then built based on these genes, with model parameters optimized through stepwise regression. Each patient's risk score was calculated, and patients were classified into high-risk and low-risk groups according to the median risk score. Additionally, the model's survival prediction efficacy was validated in both the testing set and an independent GEO dataset, with ROC curves employed to evaluate prognostic performance. The risk model's predictive ability was also explored across different clinical subgroups. The risk score formula of the model is: Risk_Score = Σ (Expression_Level of Gene_i × Coefficient_i). (Model coefficients are shown in Supplementary Table 1).

The prognostic model was further evaluated in terms of clinical relevance and practical application value. By combining the risk score with clinical characteristics, a nomogram was constructed to quantify individualized prognostic prediction. The consistency between the prediction results and the actual survival data and the discrimination ability of the model were quantitatively evaluated by calibration curves and C-index. Decision curve analysis (DCA) and time-dependent ROC curves were used to comprehensively evaluate the clinical practicability and accuracy of the nomogram model and various clinical characteristics in predicting survival outcomes at specific time points (such as advanced patients), providing more intuitive and reliable reference bases for clinical decision-making.

2.4 Immune characteristics and functional enrichment analysis

The molecular mechanisms of the risk score and its relationship with immune-related features are of great significance for revealing the biological basis of tumors and enabling precision treatment. In this study, taking the association and

difference between the risk score and immune checkpoint-related genes as the entry point, the gene expression levels of the high-risk and low-risk groups were compared. From an immunological perspective, the interactive relationship between the risk score and the tumor immune microenvironment was analyzed, the interactions among immune cells and their connections with the risk score were clarified, and the distribution differences of immune cells in different risk groups were evaluated. Furthermore, the Gene Set Enrichment Analysis (GSEA) method was employed to focus on KEGG pathways and GO biological functions, and pathways and functional modules with significant enrichment ($p < 0.05$) were screened out.

2.5 Immune therapy evaluation and tumor mutational burden analysis

Aiming to uncover the relationship between the risk score and the immune as well as mutation characteristics of tumors, this study analyzed the response patterns of patients at different risk levels to immune checkpoint inhibitor (ICI) treatment based on The Cancer Immunome Atlas (TCIA) database, with particular emphasis on four categories of immune treatment score (IPS), namely CTLA4-negative/PD1-negative, CTLA4-negative/PD1-positive, CTLA4-positive/PD1-negative, and CTLA4-positive/PD1-positive. In conjunction with the analysis of tumor mutation burden (TMB), patients were categorized into high-TMB and low-TMB groups by optimizing the cutoff value, and comprehensive groups (such as H-TMB + high-risk group, L-TMB + low-risk group) were established based on the risk score. Survival analysis indicated that significant differences existed in the survival outcomes of patients in different groups, thereby revealing the synergistic role of TMB and the risk score in prognostic assessment. Furthermore, by integrating the risk score, TMB, microsatellite instability (MSI), and immune cell infiltration characteristics, the potential associations between these molecular characteristics and the risk score were quantified through correlation analysis.

2.6 External database validation

To thoroughly explore the potential of biological markers of the key prognostic LMRGs, this study utilized the Kaplan–Meier Plotter database (https://kmplot.com/analysis/) [19] to conduct survival analysis on the screened key prognostic genes (PDGFRL, APLNR, THRB, PRKCQ, STAT2), and evaluate the relationship between the expression levels of these genes and the overall survival (OS) of patients.

2.7 Statistical analysis

All statistical analyses were completed in R software (version 4.2.1). The preliminary collation and cleansing of the raw data were accomplished by Perl scripts. The differences in gene expression were analyzed using the Wilcoxon rank-sum test, with the screening criteria set as logFC > 1 and FDR < 0.05. Survival analysis was conducted via the Kaplan–Meier method, and the log-rank test was employed to evaluate the differences between groups. The differences in immune cell infiltration between the high-risk and low-risk groups were analyzed by the Wilcoxon rank-sum test. The correlation between the immune cell infiltration level and TMB was calculated through Pearson correlation analysis, with the significance level set at $p < 0.05$. All statistical tests were two-sided tests.

3 Results

3.1 Expression Trends of LMRGs and NMF Analysis

Figure 1A presents a Venn diagram illustrating the union of immune-related genes and lactate metabolism genes. Based on the determined screening thresholds, lactate metabolism and immune-related genes were screened, and a total of 801 LMRGs were included (Supplementary Table 2). A heatmap presented the significantly differential expression of the top 50 LMRGs with the most significant differences in normal tissues and tumor tissues (Fig. 1B). A volcano plot identified the separation trend of up-regulated and down-regulated genes from non-significant genes, revealing the overall trend of gene expression changes (Fig. 1C). The results of the NMF clustering analysis showed that the consensus matrix effectively divided the samples into two tumor subtypes (Fig. 1D). By evaluating the consensus coefficient, residual, dispersion, and silhouette coefficient, the optimal decomposition rank (K = 2) was determined, validating the stability and

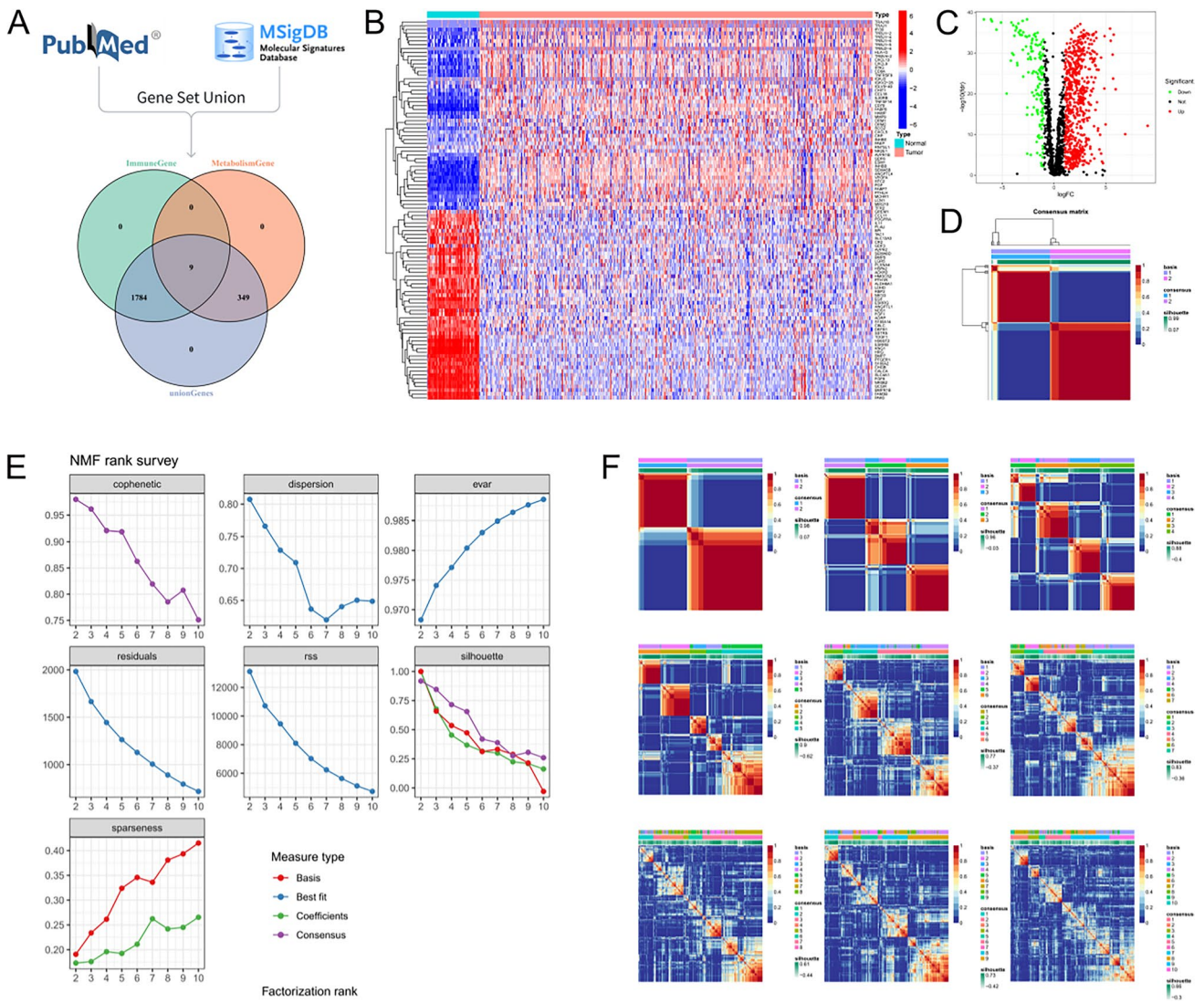

Fig. 1 Comprehensive analysis of LMRGs in tumor and normal tissues. **A** Screening of the union of immune-related genes and lactate metabolism-related genes. **B** The heatmap presents the expression status of the top 50 LMRGs with the most significant differences in tumor tissues and normal tissues. **C** The volcano plot demonstrates the distribution of differentially expressed genes. **D** The NMF consensus matrix divides the tumor samples into two molecular subtypes. **E** The evaluation results of the NMF decomposition rank show that the optimal decomposition rank is K = 2. **F** The consensus matrices under different decomposition rank further verify the classification reliability of K = 2

accuracy of the clustering (Fig. 1E). In addition, the consensus matrices at different ranks exhibited a clear block structure (Fig. 1F), further confirming the reliability of the classification of the two tumor subtypes.

3.2 Tumor Subtype Identification and Tumor Microenvironment Characterization

To better disclose tumor heterogeneity and explore the expression patterns of LMRGs between the two typing subtypes, a heatmap demonstrated that there were significant differential expressions of LMRGs in the two types (Fig. 2A). Kaplan–Meier survival curve analysis indicated that (Fig. 2B-C) the OS and PFS of patients in Cluster 2 were significantly higher than those of patients in Cluster 1 ($p < 0.001$). The results of principal component analysis (PCA) further confirmed that the two types exhibited significant separation in spatial distribution (Fig. 2D).

Tumor microenvironment (TME) score analysis revealed that the StromalScore, ImmuneScore, and ESTIMATEScore of Cluster 2 were all significantly lower than those of Cluster 1 (Fig. 2E). This suggests that there are significant differences in the composition of the TME between the two groups. The tumor microenvironment of Cluster 1 may possess richer

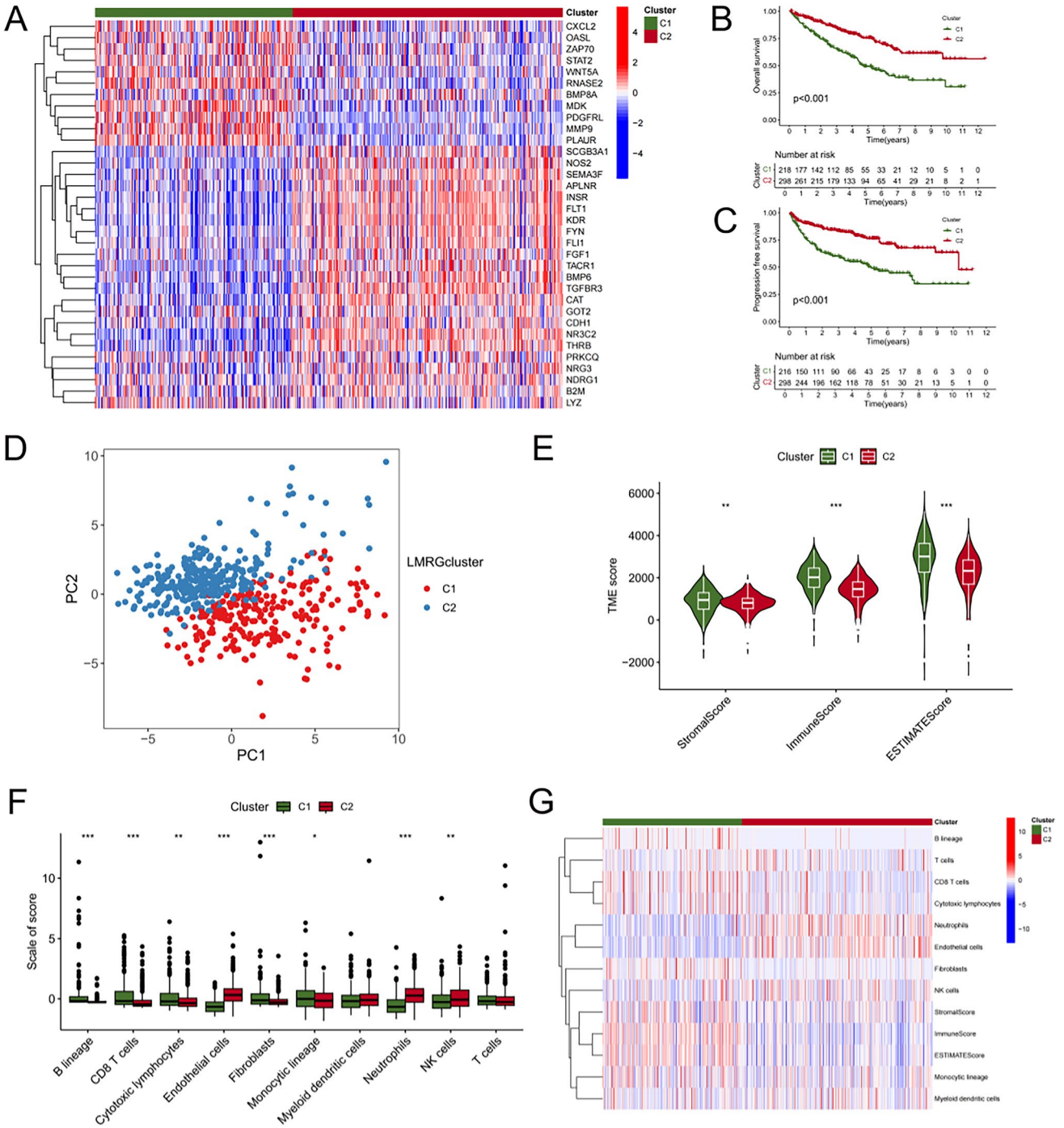

Fig. 2 Expression patterns, prognosis, and TME analysis between LMRG subtypes. **A** The heatmap displays the significant differential expressions of LMRGs in the two subtypes. **B**, **C** The Kaplan–Meier survival analysis shows the OS and PFS of patients between the two subtypes. **D** PCA shows the differences in spatial distribution between the two subtypes. **E** The TME score analysis presents the distributions of StromalScore, ImmuneScore, and ESTIMATEScore of the two subtypes. **F** The immune cell infiltration analysis demonstrates the differences in the infiltration levels of different immune cells in the two subtypes. **G** The heatmap shows the distributions of immune cell subsets and TME scores in patients of the two subtypes

stromal and immune components, thereby resulting in differences in the prognosis of patients between the two groups. The results of immune cell infiltration analysis found that the infiltration degrees of B lineage, CD8 T cells, cytotoxic lymphocytes, fibroblasts, and monocytic lineage in Cluster 1 were significantly higher than those in Cluster 2; conversely, the infiltration degrees of endothelial cells, neutrophils, and NK cells were higher in Cluster 2 (Fig. 2F). The heatmap of

immune cell infiltration (Fig. 2G) further presented the distribution of different immune cell subsets and TME scores in the two groups of samples, comprehensively revealing the significant differences in the immune microenvironment between the tumor subtypes.

3.3 LASSO Regression for key gene selection and prognostic value analysis

Via LASSO regression analysis, we screened out five LMRGs (STAT2, PDGFRL, APLNR, PRKCQ, and THRB) that were significantly associated with prognosis. The LASSO regression coefficient path diagram demonstrated that with the increase of the regularization parameter λ, the regression coefficients of most genes were gradually compressed to 0, leaving only the key genes (Fig. 3A). Cross-validation determined the optimal λ value, which balanced the complexity and prediction performance of the model (Fig. 3B). The bar chart presented the regression coefficients of each gene, among which STAT2 and PDGFRL were associated with high risk, while APLNR, PRKCQ, and THRB were associated with low risk (Fig. 3C). The Kaplan–Meier survival curve further validated the effectiveness of the model. The results showed that the survival rate of patients in the high-risk group was significantly lower than that in the low-risk group, and the difference was statistically significant ($p < 0.05$, Fig. 3D–G). The ROC curve evaluated the prediction accuracy of the model. Except for the 5-year AUC value of the validation set being 0.676, the AUC values of the other datasets at 1 year, 3 years, and 5 years all exceeded 0.7, indicating that the model had good prediction performance and robustness (Fig. 3H–J). The risk distribution map and survival status scatter plot (Fig. 3L, Supplementary Fig. 2) indicated that death events were mainly concentrated in high-risk patients, and the survival time shortened as the risk score increased. The gene expression heatmap disclosed the differences in molecular characteristics between the high-risk and low-risk groups. Among them, STAT2 and PDGFRL were highly expressed in the high-risk group, while APLNR, PRKCQ, and THRB were highly expressed in the low-risk group.

3.4 Clinical evaluation of the prognostic model's utility

The results of the Kaplan–Meier survival analysis demonstrated that the survival rate of patients in the high-risk group was significantly lower than that in the low-risk group, and this trend was manifested in both early-stage and late-stage patients (Fig. 4A, B). The nomogram constructed based on age, gender, risk score, and stage (Fig. 4C) could effectively predict the survival probabilities of patients at 1 year, 3 years, and 5 years, among which the risk score and stage had greater weights. The calibration curve revealed that the prediction results of the nomogram were highly consistent with the actual observations, with the C-index reaching 0.778 (Fig. 4D), indicating that the model had good prediction performance. ROC curve analysis validated the superiority of the nomogram. Its AUC value was 0.769, which was significantly higher than that of a single variable, indicating that the model after integrating multiple factors had higher prediction accuracy (Fig. 4E). Decision curve analysis indicated that the nomogram had the highest clinical net benefit under different risk thresholds and was superior to other variables (Fig. 4F), further demonstrating its clinical practicability. The results of Cox regression analysis indicated that the risk score, stage, and age were important factors affecting survival. In the univariate analysis, the risk score and stage were significantly associated with survival risk (Fig. 4G). Multivariate analysis further confirmed that the risk score and stage were independent prognostic factors (Fig. 4H).

3.5 Immune microenvironment and functional analysis

The correlation analysis of immune checkpoint genes revealed that the risk score was positively correlated with PDCD1, CTLA4, POLE2, FAP, and LOXL2, while negatively correlated with MSH2 and TAGLN (Fig. 5A). The box plot further validated the differential expression of genes. The results demonstrated that CTLA4, FEN1, and PDCD1 were significantly upregulated in the high-risk group, while MSH2 and MSH6 were significantly upregulated in the low-risk group (Supplementary Fig. 2A-L).

The correlation analysis of immune cell infiltration indicated that the risk score was significantly positively correlated with CD8 + T cells, B lineage, Monocytic lineage, and Fibroblasts, while negatively correlated with Neutrophils and Endothelial cells (Fig. 5B). The violin plot confirmed this result and further disclosed that Cytotoxic lymphocytes were significantly enriched in the high-risk group (Supplementary Fig. 3A-J).

The GSEA analysis demonstrated that there were significant differences in functions and pathways among different risk groups. Based on the GO gene set, the high-risk group was enriched in immune-related functions such as antigen recognition, immune receptor binding, and immune activation (Fig. 5C), while the low-risk group was enriched in metabolism-related functions such as transmembrane transport, metal ion transport, and enzyme activity regulation

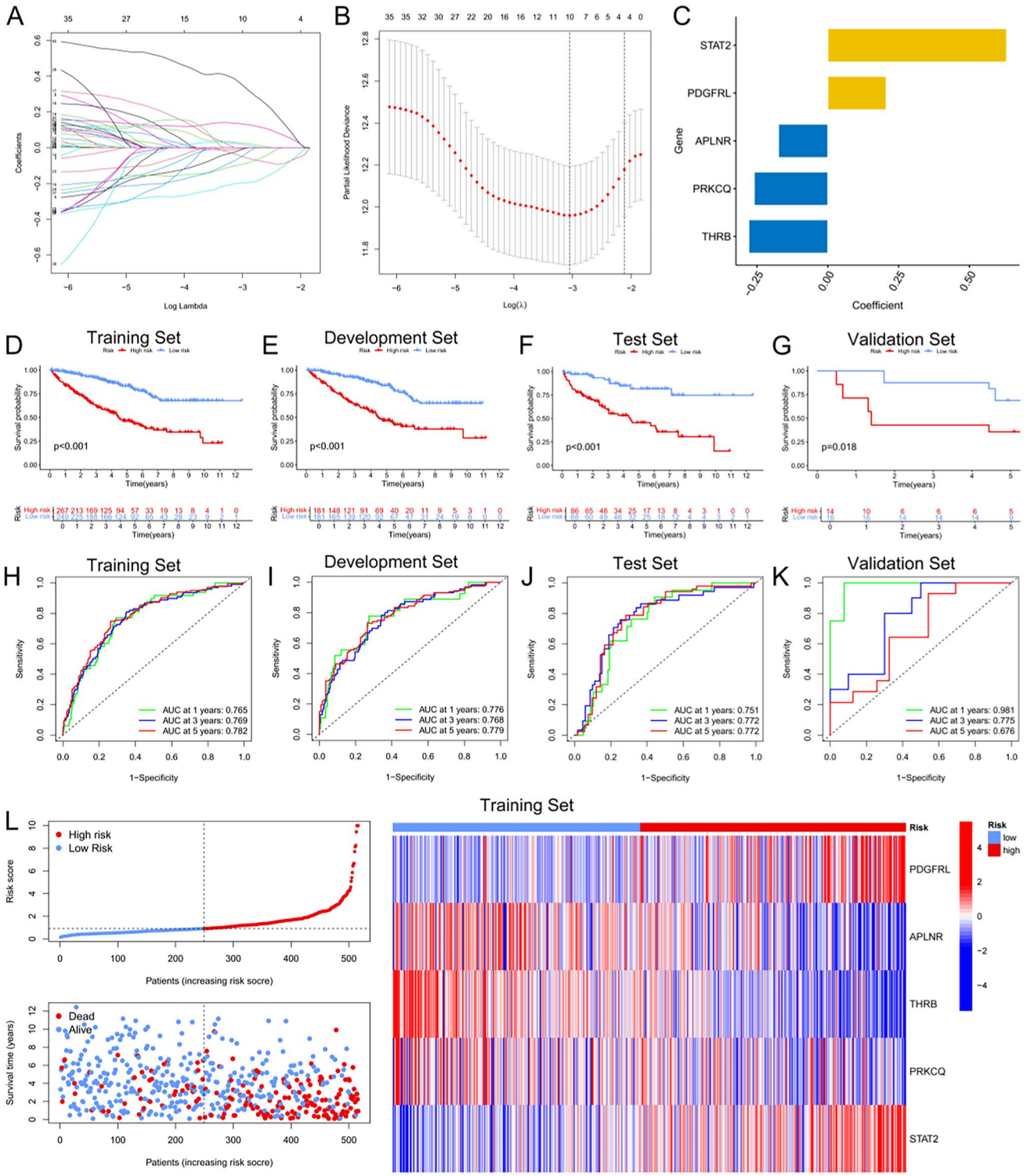

Fig. 3 Screening of key genes by LASSO regression and their prognostic analysis. **A** The LASSO regression coefficient path diagram. **B** Cross-validation determines the optimal λ value. **C** The bar chart of the five screened key genes and their regression coefficients. **D**–**G** The Kaplan–Meier survival curves show the survival differences between patients in the high-risk and low-risk groups. **H**–**J** The ROC curves evaluate the survival prediction ability of the model. **K** The ROC curve of the validation set. **L** The risk score distribution map, survival status scatter plot, and gene expression heatmap show the characteristic differences between the high-risk and low-risk groups in the training set

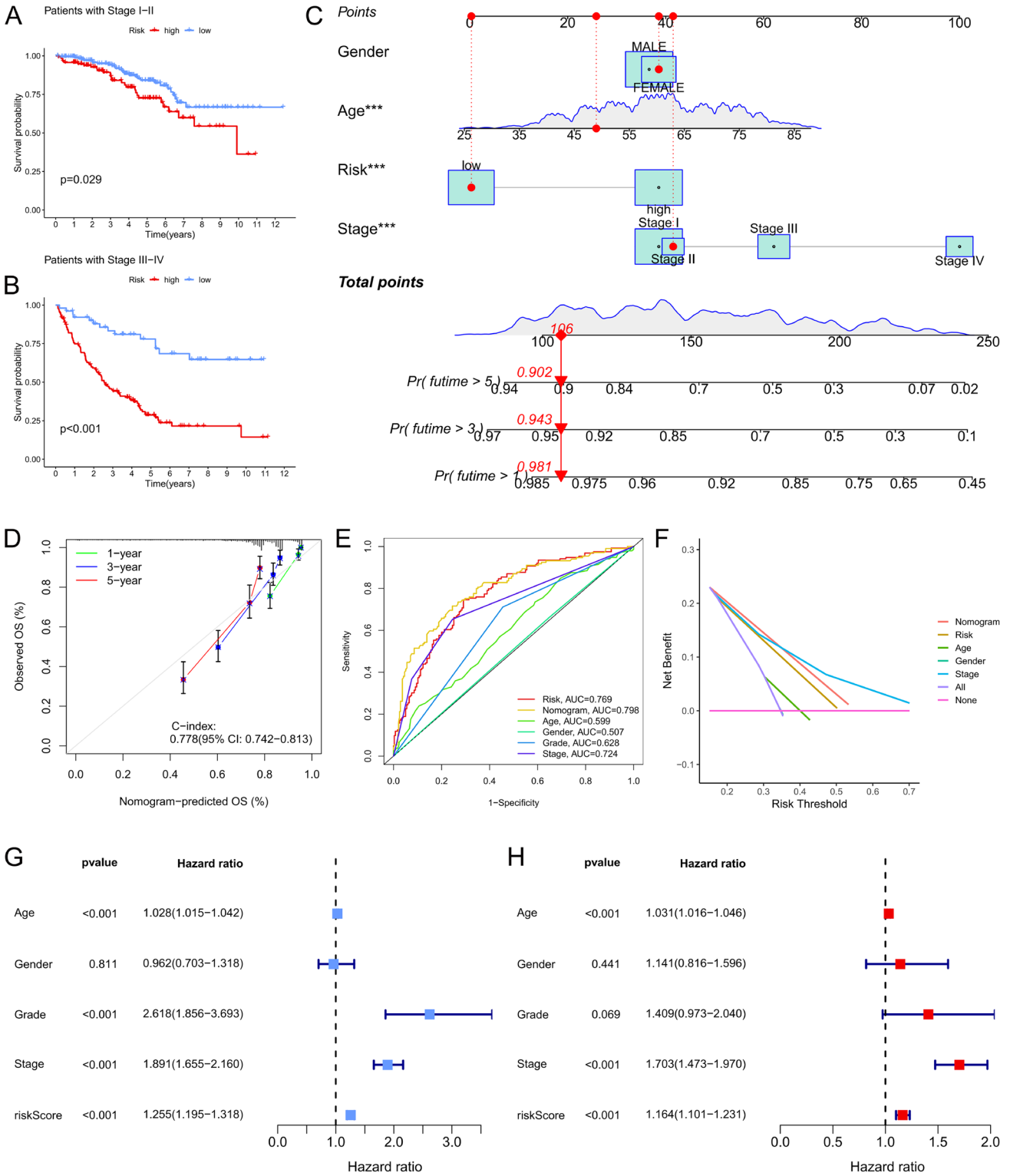

Fig. 4 Construction of the prognostic model and evaluation of its clinical value. **A**, **B** The survival curves of patients in the high-risk and low-risk groups in the early and late stages. **C** The nomogram is constructed based on age, gender, stage, and risk score. **D** The calibration curve of the nomogram. **E** The ROC curve evaluates the prediction performance of the nomogram. **F** The decision curve analysis shows the clinical net benefits of different variables and the nomogram under various risk thresholds. **G**, **H** The univariate and multivariate Cox regression analyses show the impacts of different variables on survival risk

Discover Oncology (2025) 16:1024 | https://doi.org/10.1007/s12672-025-02746-2

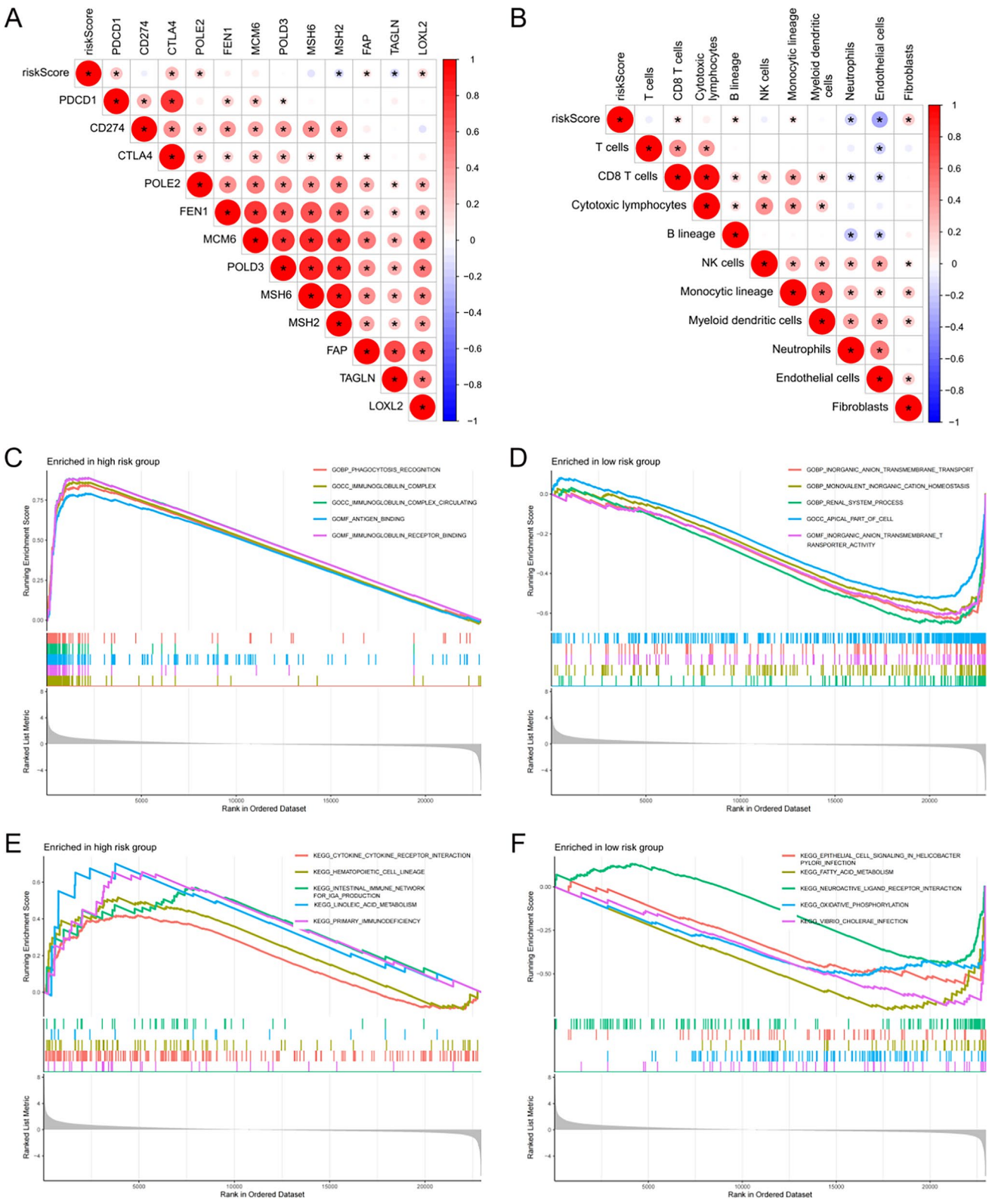

Fig. 5 Analysis of the immune microenvironment and functions. **A** The correlation heatmap between the risk score and immune checkpoint genes. **B** The correlation heatmap between the risk score and immune cell infiltration. **C**, **D** The GSEA based on the GO gene set shows the differences in functional enrichment between the high-risk and low-risk groups. **E**, **F** The GSEA based on the KEGG gene set shows the differences in pathway enrichment between the high-risk and low-risk groups

(Fig. 5D). Based on the KEGG gene set, the high-risk group was enriched in immune pathways such as cytokine-receptor interaction and natural killer cell-mediated cytotoxicity (Fig. 5E). The low-risk group, on the other hand, was enriched in metabolism and signal transduction pathways such as oxidative phosphorylation, calcium signaling pathway, and cell adhesion molecules pathways (Fig. 5F).

3.6 Combined analysis of immunotherapy and TMB

The TCIA analysis revealed that there were differences in the IPS between the high-risk and low-risk groups. The scores of CTLA4_neg_PD1_neg and CTLA4_pos_PD1_pos were significantly increased in the high-risk group ($p < 0.05$, Fig. 7A, D). However, the scores of CTLA4_neg_PD1_pos and CTLA4_pos_PD1_neg showed no significant differences between the two groups (Fig. 7B, C). The chord diagram indicated that the risk score was positively correlated with TMB, but TMB was negatively correlated with immune cell infiltration (Fig. 6E). Specifically, CD8 T cells were positively correlated with Cytotoxic lymphocytes but negatively correlated with TMB; meanwhile, Endothelial cell was also positively correlated with Neutrophils but negatively correlated with TMB. The results of the survival analysis demonstrated that the survival

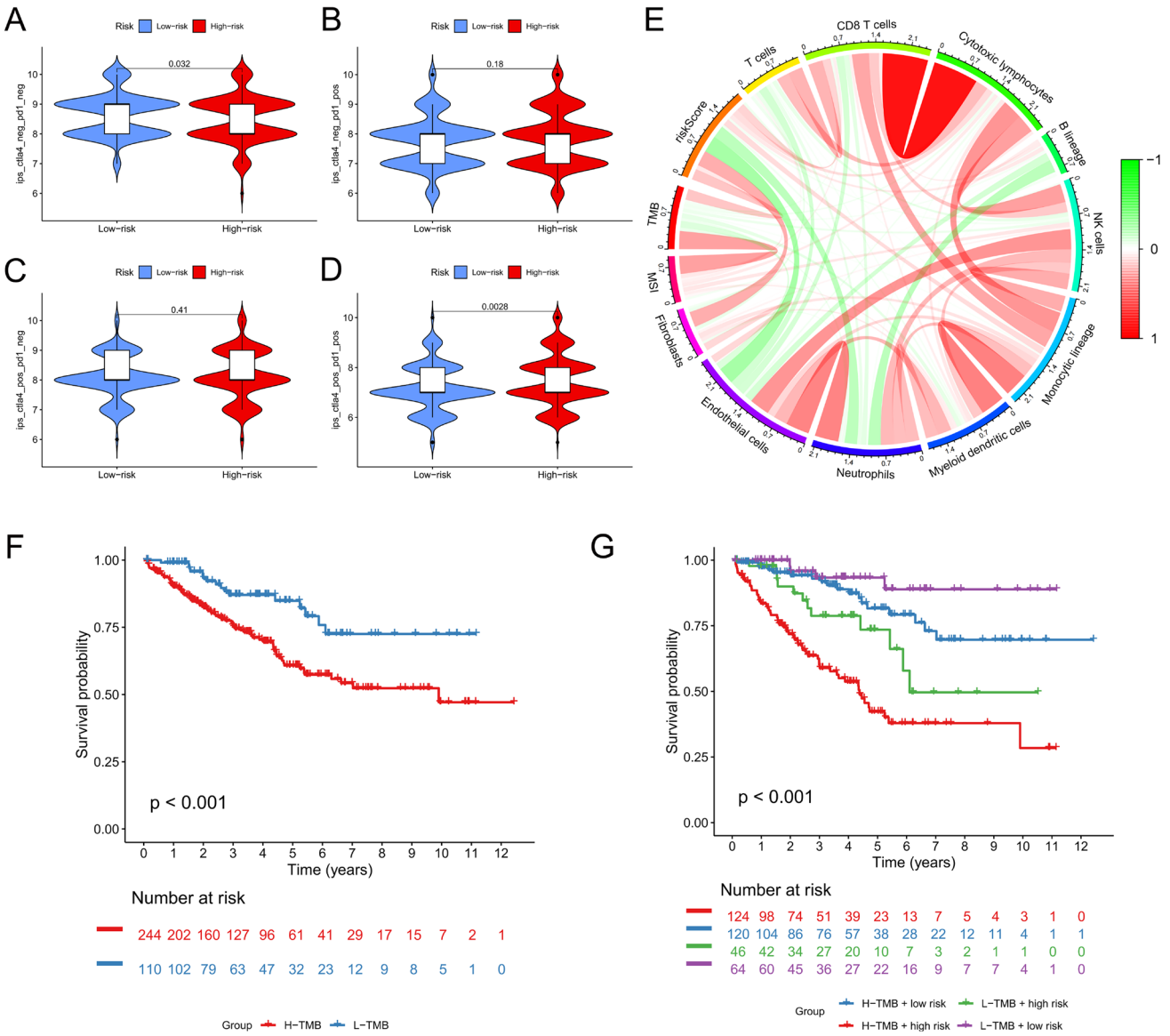

Fig. 6 Combined analysis of the IPS and TMB. **A**–**D** The differences of different IPS between the high-risk and low-risk groups. **E** The correlations among the risk score, TMB, and immune cell infiltration. **F** The survival differences between patients in the high-TMB group and the low-TMB group. **G** The survival analysis combines TMB and the risk score

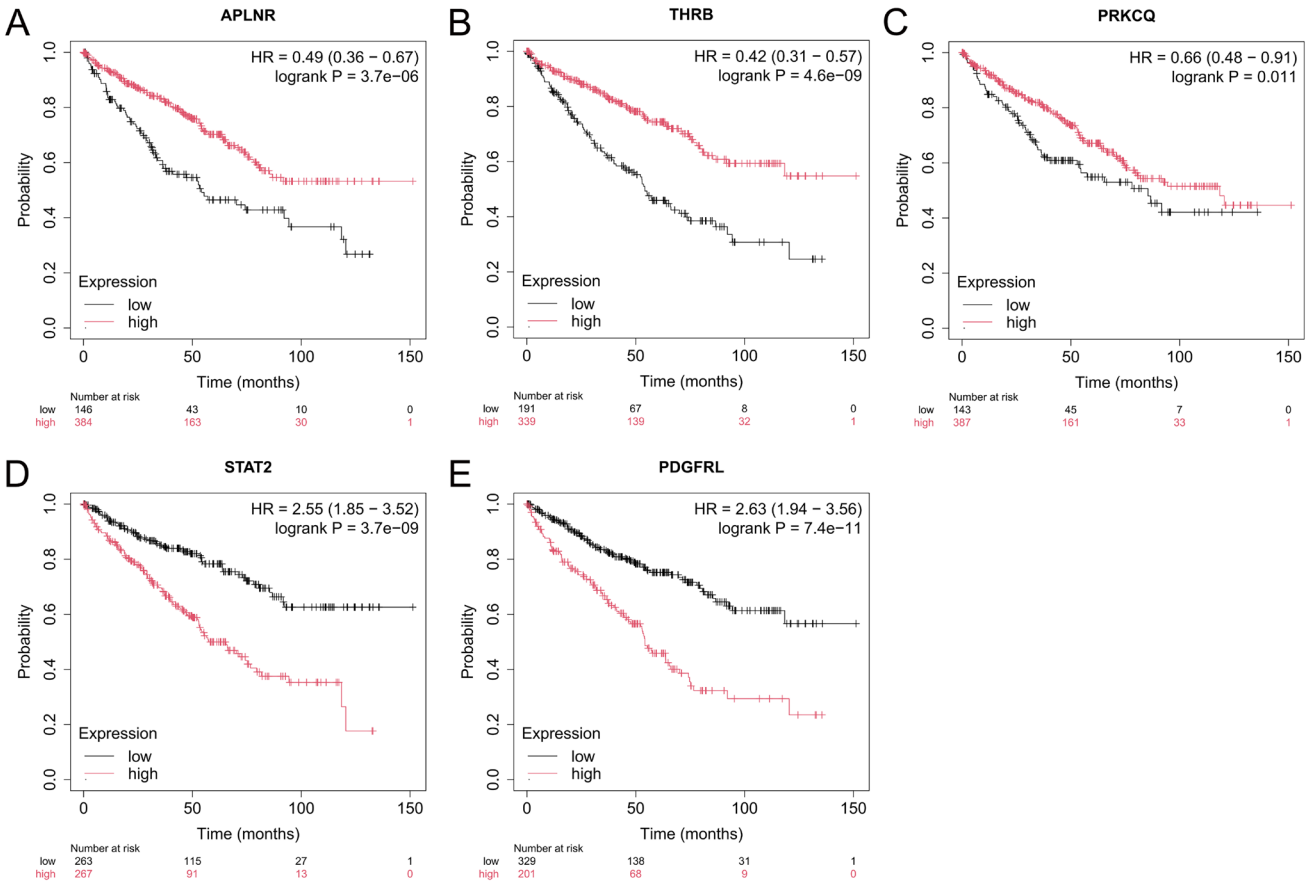

Fig. 7 Survival analysis of the core LMRGs based on the K – M database. **A**–**E** The relationships between the expression levels of different core LMRGs (APLNR, THRB, PRKCQ, STAT2, PDGFRL) and the survival time of patients

rate of patients in the high-TMB group was significantly lower than that in the low-TMB group ($p < 0.001$, Fig. 6F). After the combined analysis of TMB and the risk score, the survival rate of the H-TMB + high-risk group was the lowest, while that of the L-TMB + low-risk group was the highest (Fig. 6G). This result indicates that TMB and the risk score have a synergistic effect and can evaluate the survival prognosis of patients more effectively.

3.7 Prognostic validation of core LMRGs BASED on the Kaplan–Meier database

Survival analysis based on the Kaplan–Meier (K-M) database demonstrated that the high expression of APLNR, THRB, and PRKCQ significantly prolonged the survival time (with hazard ratios (HR) of 0.49, 0.42, and 0.66 respectively, $p < 0.05$), while the high expression of PDGFRL and STAT2 significantly shortened the survival time (with HRs of 2.63 and 2.55 respectively, $p < 0.001$). These results validated the prognostic value of the core LMRGs.

4 Discussion

In recent years, immunotherapy represented by immune checkpoint inhibitors (ICIs) has become a pivotal strategy for treating ccRCC, a tumor characterized by high immunogenicity but poor response to conventional chemotherapy [20]. ICIs restore T cell function and activate the anti-tumor immune response by blocking immune checkpoint pathways such as PD - 1/PD - L1 and CTLA - 4 [21, 22]. However, due to the immunosuppressive TME characteristic of ccRCC, the efficacy of ICIs remains limited in many patients. The immunosuppressive state in the TME is driven by multiple factors, including the high expression of immune checkpoint molecules, the remodeling of the tumor stroma, and the accumulation of metabolites, among which the enhancement of lactate metabolism is particularly crucial [23, 24]. Recent multi-omics and urine-based metabolomic studies have demonstrated that high-grade ccRCC exhibits enhanced glycolysis, impaired

oxidative phosphorylation, and lipid metabolic shifts. Elevated urinary lactate and pyruvate levels, together with transcriptomic changes in $CD133^+/CD24^+$ tumor stem cells, reflect a HIF-α–driven activation of glycolytic and acetyl-CoA biosynthetic pathways, in part mediated by NDUFA4L2-induced inhibition of mitochondrial Complex I and metabolic rerouting toward the pentose phosphate pathway [7, 25, 26]. Lactate, a central byproduct of this reprogramming, not only suppresses $CD8^+$ T cell activity and promotes Treg and TAM differentiation, but also facilitates epithelial–mesenchymal transition via SIRT1/SMAD4-mediated epigenetic regulation [6]. Grade-stratified functional studies confirmed that metabolic dependencies in ccRCC differ by tumor grade, with high-grade tumors exhibiting enhanced reliance on glycolysis and fatty acid oxidation [27].

This investigation systematically explored the potential roles and prognostic values of LMRGs in ccRCC and disclosed the possible associations between lactate metabolism and immune regulation in tumor progression. Via NMF clustering analysis, ccRCC patients were divided into two subtypes based on the differential gene expression data of LMRGs. It is noteworthy that the term "cytotoxic lymphocytes" encompasses not only $CD8^+$ T cells but also other cell types such as natural killer cells, which play a crucial role in tumor immune surveillance. Our study found that, although the C1 group exhibited higher infiltration levels of $CD8^+$ T cells and CLs, these patients had poorer survival outcomes. Generally, $CD8^+$ T cells are associated with antitumor activity; however, in an immunosuppressive microenvironment—shaped by various factors such as TGF-β signaling or complement-related inflammation—low-activity or dysfunctional $CD8^+$ T cells, even when abundant, may fail to exert effective cytotoxic function [28–31]. This dysfunction is further reinforced by metabolic factors; lactate and succinate stabilize HIF-α and inhibit α-ketoglutarate-dependent dioxygenases, suppressing T cell activity and promoting immune evasion in ccRCC [32].

Furthermore, the role of regulatory T cells (Tregs) in the tumor microenvironment (TME) is significant. Tregs secrete immunosuppressive factors (e.g., IL-10 and TGF-β) that inhibit the activity of effector T cells, thereby exacerbating the immunosuppressive state and facilitating tumor immune evasion [33]. Additionally, the C1 group demonstrated higher levels of fibroblast infiltration. Research suggests that tumor-associated fibroblasts may secrete TGF-β and other paracrine signals to promote epithelial-mesenchymal transition (EMT) in tumor cells, potentially impacting both immune cell infiltration and cytotoxic function [34]. TGF-β also enhances ccRCC invasiveness by promoting ROS-mediated Abl2 degradation and invadopodia maturation, thereby facilitating tumor cell migration and extracellular matrix degradation [35]. In contrast, although the C2 group showed lower levels of $CD8^+$ T cells and CLs, it exhibited higher endothelial cell infiltration. This increased endothelial presence may enhance vascular permeability, thereby improving immune cell extravasation and strengthening local immune responses [36]. Moreover, the C2 group had elevated neutrophil levels. While neutrophils can promote immune suppression in some cancers, they may, under certain conditions, enhance immune cell activation through increased inflammation or the release of chemotactic factors, thus influencing patient prognosis [37]. Consequently, the tumor microenvironment in the C2 group may be more favorable for effective immune responses, which could explain the observed better survival outcomes.

Further analysis revealed that the StromalScore, ImmuneScore, and ESTIMATEScore in the C1 group were significantly higher than those in the C2 group, indicating a greater infiltration of immune cells and stromal components in the TME of the C1 group. However, higher infiltration does not necessarily correlate with effective antitumor immunity. The poorer prognosis observed in the C1 group may be attributed to an excessive presence of stromal elements (e.g., fibroblasts) that impair immune cell function, an uneven distribution of immune cells, or the altered expression of certain immunoregulatory factors [34].

Via Cox regression analysis and machine learning algorithm (LASSO regression), five core genes significantly associated with patient prognosis were screened out based on the differential expression of LMRGs: STAT2, PDGFRL, APLNR, PRKCQ, and THRB. Notably, the gene set after NMF typing contained the key prognostic genes, indicating that the typing results not only revealed the molecular subtype characteristics of patients but also had a high degree of consistency with the screening results of the core genes in biological significance. Further functional analysis of the core genes demonstrated that these genes may play crucial roles in metabolism and immune regulation. STAT2 is a key transcription factor in the interferon signaling pathway that is significantly upregulated in ccRCC and closely associated with poor prognosis [38]. High STAT2 expression may promote immune evasion and tumor progression by activating downstream immune regulatory and cell proliferation-related genes, and it may also be involved in regulating drug resistance [38, 39]. These findings support STAT2 as a potential biomarker for ccRCC prognosis and suggest that its roles in tumor immunity and therapeutic resistance warrant further investigation. In ccRCC, our study found that PDGFRL is significantly upregulated and exhibits oncogenic properties. Although we have not performed separate immune and metabolic subgroup analyses for PDGFRL, the literature indicates that its function in different tumors is highly dependent on the microenvironment. For instance, in gastric cancer, PDGFRL upregulation is closely associated with tumor progression, suppression of T cell

antigen presentation, and reduced MHC I expression, thereby promoting immune evasion [40]. In contrast, in hepatocellular carcinoma, PDGFRL acts as a tumor suppressor by inhibiting proliferation and inducing apoptosis, correlating with poor prognosis [41]. These discrepancies indicate that PDGFRL function is modulated by both the tumor microenvironment and molecular context. Future research into the association between PDGFRL, tumor immunity, and metabolism will provide a robust molecular basis for elucidating its role in ccRCC and developing targeted therapies.

APLNR is significantly upregulated in low-risk ccRCC patients, potentially by maintaining metabolic homeostasis and reducing tumor cell reliance on aberrant metabolic pathways, thereby inhibiting tumor progression [42]. Furthermore, a stable metabolic state supports effective antitumor immune responses, leading to improved patient outcomes [43]. High THRB expression is associated with better prognosis in ccRCC patients. As thyroid hormone receptor β, THRB plays a crucial role in regulating cellular metabolism and mitochondrial function; its activation helps sustain oxidative phosphorylation, thereby inhibiting metabolic reprogramming and tumor cell proliferation [44, 45]. In addition, a stable metabolic state supplies immune cells with sufficient energy, supporting their antitumor activity [46]. Thus, high THRB expression not only enhances tumor cell metabolic balance but may also indirectly bolster antitumor immunity. Previous studies have indicated that PRKCQ is involved in regulating cell motility and proliferation, and it may also be closely linked to cellular metabolism and inflammatory responses. In our study, PRKCQ was upregulated in low-risk patients. Although its specific mechanisms in immune and metabolic regulation remain incompletely understood, some evidence suggests that PRKCQ may help maintain cellular homeostasis by coordinately modulating metabolism and inflammatory responses, thereby limiting tumor invasion and metastasis [47]. Overall, the functional characteristics of these core genes further elucidate the complex interplay between metabolic regulation and immune modulation in ccRCC, providing a robust molecular basis for constructing precise prognostic models and developing personalized therapeutic strategies.

In the high-risk group, the tumor microenvironment exhibited significant activation of immune checkpoint molecules, with notably elevated expression of PDCD1, CTLA-4, and FAP. The overexpression of PD-1 and CTLA-4 may inhibit T cell function, thereby weakening antitumor immune responses and facilitating tumor immune evasion. Co-expression of PD-1 with other inhibitory receptors such as TIM-3 has also been associated with more aggressive phenotypes and worse prognosis in ccRCC [48, 49]. Concurrently, FAP upregulation suggests enhanced tumor matrix remodeling and fibrosis; previous studies have demonstrated that interventions targeting FAP can not only improve the penetration of conventional immunosuppressants into tumor tissues but also reduce the protumor effects of cancer-associated fibroblasts [50]. Although the high-risk group exhibited higher infiltration levels of cytotoxic lymphocytes and $CD8^+$ T cells, these immune cells are often rendered functionally exhausted due to persistent activation by immunosuppressive factors and checkpoint molecules within the tumor microenvironment, impairing their ability to recognize and eliminate tumor cells. This phenomenon reflects a complex mechanism in which immune suppression coexists with functional exhaustion [12, 28]. Overexpression of MUC1 in ccRCC is associated with complement activation, enrichment of M2-type TAMs and $IDO1^+$ cells, and reduced $CD8^+$ T cell infiltration, indicating an immune-silent microenvironment with impaired cytotoxic activity [51, 52]. Notably, MUC1-associated PTX3 overexpression activates the complement cascade (C1q, C3aR, C5aR1) while upregulating CD59 to limit terminal cytolysis, thereby facilitating angiogenesis and immune escape [53]. It also contributes to metabolic reprogramming, including enhanced pentose phosphate pathway activity, glutathione accumulation, and suppression of mitochondrial ROS, collectively facilitating immune evasion and chemoresistance [54–56]. Moreover, gene enrichment analyses revealed that pathways related to antigen recognition, immune receptor binding, and immune activation are enriched in the high-risk group. Although these findings suggest that the immune system is activated to some extent, they more likely indicate an "activated yet inefficient" state, wherein compensatory immune activation is offset by the inhibitory effects of factors such as TGF-β and IL-10, as well as immune checkpoint molecules, ultimately limiting cytotoxic function and resulting in poor patient outcomes [30, 34]. In contrast, patients in the low-risk group exhibited more balanced and effective immune and metabolic characteristics, potentially benefiting from a metabolically favorable tumor microenvironment. Previous studies have shown that glycolytic overactivation and TCA cycle suppression can impair T cell function and hinder immunotherapeutic efficacy [57]. In our study, low-risk patients also exhibited significantly downregulated immune checkpoint expression and upregulated DNA repair-related genes (e.g., MSH2 and MSH6), which may contribute to improved genomic stability and reduced tumor aggressiveness [58].

In our study, tumors from low-risk patients demonstrated enrichment of oxidative phosphorylation, calcium signaling pathways, and cell adhesion molecules, among other metabolic and signal transduction pathways [59, 60]. Although numerous studies have reported that these pathways can enhance tumor cell proliferation, migration, and metastasis in certain contexts [61, 62], our data show that the upregulation of these pathways coexists with higher expression of DNA repair-related genes, suggesting that the low-risk group may maintain a relatively stable and well-differentiated metabolic state. In other words, within the specific context of ccRCC, the activation of these metabolic pathways may

reflect more complete metabolic regulation and lower genomic instability in tumor cells, thereby delaying malignant progression [63]. We propose that the impact of metabolic activity is highly dependent on the tumor microenvironment and its overall molecular characteristics. Therefore, in this study, the metabolic advantages observed in the low-risk group are closely associated with favorable prognosis, whereas the high-risk group is characterized primarily by immune suppression and exhaustion, providing a basis for the development of precise therapeutic strategies.

The results of TMB analysis demonstrated that CD8 + T cells and cytotoxic lymphocytes were negatively correlated in patients with high TMB, suggesting that a high mutation burden might limit the functional anti-tumor effect of T cells by inducing an immunosuppressive tumor microenvironment [64]. Conversely, endothelial cells and Neutrophils were positively correlated with TMB, which might reflect that high mutation burden promoted the enhancement of angiogenesis and inflammatory response [65]. The results of survival analysis further indicated that the overall survival rate of patients in the high-TMB group was significantly lower than that in the low-TMB group, suggesting that a high mutation burden might be closely associated with a poorer prognosis.

The results of the ROC curve and DCA demonstrated that the risk score model exhibited good performance in survival prediction at 1 year, 3 years, and 5 years, reflecting its robustness in short-term and long-term prognostic assessment. In addition, the nomogram constructed by combining the risk score with clinical features (such as stage and age) effectively quantified the individualized survival probability, further highlighting the potential value of the model in clinical application.

Although this study employed multi-omics analysis using public databases from TCGA and GEO to construct a prognostic risk scoring model and elucidate the critical roles of lactate metabolism and immune regulation in ccRCC, several limitations remain. First, our data were primarily derived from public databases and lack validation from an independent external cohort, potentially limiting the generalizability of the model across diverse populations. Second, although key genes in the high-risk group were identified through NMF subtyping and LASSO regression, the specific biological mechanisms underlying their roles in lactate metabolism and immune evasion have not been thoroughly investigated in vitro or in vivo. Third, our functional enrichment analysis relied mainly on transcriptomic data without integrating proteomic or metabolomic information, which may be insufficient to fully capture the dynamic interplay between lactate metabolism and immune regulation. Additionally, our analysis of immunotherapy response patterns was based primarily on data from The Cancer Imaging Archive (TCIA), which might not fully reflect the actual clinical outcomes of immunotherapy. Future studies should integrate multi-omics data and validate our risk model in larger, multicenter cohorts, while also exploring combination therapeutic strategies targeting both lactate metabolism and immune regulation to provide a more robust theoretical foundation and practical guidance for precision treatment in ccRCC.

5 Conclusion

This research revealed the molecular heterogeneity of patients with ccRCC through NMF typing. Moreover, combined with machine learning algorithms, five LMRGs with independent prognostic values were screened out, and a risk score model was constructed. Thereby, the significant differences in the tumor microenvironment, immune regulation, and metabolic pathways between patients in the high-risk and low-risk groups were systematically elucidated. These results deepened the understanding of the roles of lactate metabolism and immune regulation in the tumor progression of ccRCC, provided a new theoretical basis for the stratified management and precise treatment of patients, and simultaneously offered an important direction for the exploration of combined treatment strategies based on the targets of lactate metabolism and immune regulation.

Author contributions Author contributions : Conceptualization:Jun Wu, Wenjie Zhang, Tao Zhao. Data curation: Jun Wu, Yuqian Wu. Formal analysis: Jun Wu, Yuqian Wu. Investigation: Jun Wu, Yuqian Wu, Yefeng Sun. Software: Jun Wu, Yefeng Sun, Jianhang You. Validation: Jun Wu. Visualization: Yefeng Sun, Jianhang You. Writing – original draft: Jun Wu, Yuqian Wu, Jianhang You. Writing – review & editing: Jun Wu, Yuqian Wu, Jianhang You.

Funding National Natural Science Foundation of China (82002083); Young experts of Taishan Scholars (tsqn202211380); Health Science and Technology Innovation Team Construction Project of Shandong Province (Tao Zhao).

Data availability The code supporting the findings of this study is available upon request from the corresponding author. The relevant data for this study are publicly accessible in the TCGA (https://portal.gdc.cancer.gov) and the GEO database (Access link: https://www.ncbi.nlm.nih.gov/geo/query/acc.cgi?acc=GSE167573).

Declarations

Competing interests The authors declare no competing interests.

References

1. Motzer RJ, Jonasch E, Agarwal N, et al. Kidney cancer, version 3.2022, NCCN clinical practice guidelines in oncology. J Natl Compr Canc Netw. 2022;20:71–90. https://doi.org/10.6004/jnccn.2022.0001.
2. Campbell SC, Clark PE, Chang SS, et al. Renal mass and localized renal cancer: evaluation, management, and follow-up: AUA guideline: part I. J Urol. 2021. https://doi.org/10.1097/JU.0000000000001911.
3. Ljungberg B, Albiges L, Abu-Ghanem Y, et al. European association of urology guidelines on renal cell carcinoma: the 2022 update. Eur Urol. 2022;82:399–410. https://doi.org/10.1016/j.eururo.2022.03.006.
4. Hakimi AA, Voss MH, Kuo F, et al. Transcriptomic profiling of the tumor microenvironment reveals distinct subgroups of clear cell renal cell cancer - data from a randomized phase III trial. Cancer Discov. 2019;9:510–25. https://doi.org/10.1158/2159-8290.CD-18-0957.
5. Rini BI, Plimack ER, Stus V, et al. Pembrolizumab plus axitinib versus sunitinib for advanced renal-cell carcinoma. N Engl J Med. 2019;380:1116–27. https://doi.org/10.1056/NEJMoa1816714.
6. di Meo NA, Lasorsa F, Rutigliano M, et al. Renal cell carcinoma as a metabolic disease: an update on main pathways, potential biomarkers, and therapeutic targets. Int J Mol Sci. 2022;23:14360. https://doi.org/10.3390/ijms232214360.
7. Lucarelli G, Lasorsa F, Milella M, et al. Transcriptomic and proteo-metabolic determinants of the grading system in clear cell renal cell carcinoma. Urol Oncol Semin Orig Investig. 2025. https://doi.org/10.1016/j.urolonc.2025.02.016.
8. Bombelli S, Torsello B, Marco SD, et al. 36-kDa annexin A3 isoform negatively modulates lipid storage in clear cell renal cell carcinoma cells. Am J Pathol. 2020;190:2317–26. https://doi.org/10.1016/j.ajpath.2020.08.008.
9. Lucarelli G, Galleggiante V, Rutigliano M, et al. Metabolomic profile of glycolysis and the pentose phosphate pathway identifies the central role of glucose-6-phosphate dehydrogenase in clear cell-renal cell carcinoma. Oncotarget. 2015;6:13371–86. https://doi.org/10.18632/oncotarget.3823.
10. Activation of the kynurenine pathway predicts poor outcome in patients with clear cell renal cell carcinoma - ScienceDirect. https://www.sciencedirect.com/science/article/abs/pii/S1078143917300959?via%3Dihub. Accessed 13 May 2025
11. Gigante M, Pontrelli P, Herr W, et al. miR-29b and miR-198 overexpression in CD8+ T cells of renal cell carcinoma patients down-modulates JAK3 and MCL-1 leading to immune dysfunction. J Transl Med. 2016;14:84. https://doi.org/10.1186/s12967-016-0841-9.
12. Xu W, Lu J, Liu W-R, et al. Heterogeneity in tertiary lymphoid structures predicts distinct prognosis and immune microenvironment characterizations of clear cell renal cell carcinoma. J ImmunoTher Cancer. 2023;11: e006667. https://doi.org/10.1136/jitc-2023-006667.
13. Du B, Zhou Y, Yi X, et al. Identification of immune-related cells and genes in tumor microenvironment of clear cell renal cell carcinoma. Front Oncol. 2020;10:1770. https://doi.org/10.3389/fonc.2020.01770.
14. He Z, Fischer A, Song Y, et al. Genome wide transcriptome analysis provides bases on colonic mucosal immune system development affected by colostrum feeding strategies in neonatal calves. BMC Genom. 2018;19:635. https://doi.org/10.1186/s12864-018-5017-y.
15. Subramanian A, Tamayo P, Mootha VK, et al. Gene set enrichment analysis: a knowledge-based approach for interpreting genome-wide expression profiles. Proc Natl Acad Sci USA. 2005;102:15545–50. https://doi.org/10.1073/pnas.0506580102.
16. Ritchie ME, Phipson B, Wu D, et al. limma powers differential expression analyses for RNA-sequencing and microarray studies. Nucleic Acids Res. 2015;43: e47. https://doi.org/10.1093/nar/gkv007.
17. Yoshihara K, Shahmoradgoli M, Martínez E, et al. Inferring tumour purity and stromal and immune cell admixture from expression data. Nat Commun. 2013;4:2612. https://doi.org/10.1038/ncomms3612.
18. Becht E, Giraldo NA, Lacroix L, et al. Estimating the population abundance of tissue-infiltrating immune and stromal cell populations using gene expression. Genome Biol. 2016;17:218. https://doi.org/10.1186/s13059-016-1070-5.
19. Győrffy B. Integrated analysis of public datasets for the discovery and validation of survival-associated genes in solid tumors. Innovation. 2024;5: 100625. https://doi.org/10.1016/j.xinn.2024.100625.
20. Lasorsa F, di Meo NA, Rutigliano M, et al. Immune checkpoint inhibitors in renal cell carcinoma: molecular basis and rationale for their use in clinical practice. Biomedicines. 2023;11:1071. https://doi.org/10.3390/biomedicines11041071.
21. Meng L, Collier KA, Wang P, et al. Emerging immunotherapy approaches for advanced clear cell renal cell carcinoma. Cells. 2023;13:34. https://doi.org/10.3390/cells13010034.
22. Giraldo NA, Becht E, Vano Y, et al. Tumor-infiltrating and peripheral blood T-cell immunophenotypes predict early relapse in localized clear cell renal cell carcinoma. Clin Cancer Res. 2017;23:4416–28. https://doi.org/10.1158/1078-0432.CCR-16-2848.
23. Noe JT, Rendon BE, Geller AE, et al. Lactate supports a metabolic-epigenetic link in macrophage polarization. Sci Adv. 2021;7:eabi8602. https://doi.org/10.1126/sciadv.abi8602.

24. Husain Z, Seth P, Sukhatme VP. Tumor-derived lactate and myeloid-derived suppressor cells. Oncoimmunology. 2013;2: e26383. https://doi.org/10.4161/onci.26383.
25. Ragone R, Sallustio F, Piccinonna S, et al. Renal cell carcinoma: a study through NMR-based metabolomics combined with transcriptomics. Diseases. 2016;4:7. https://doi.org/10.3390/diseases4010007.
26. Integrated multi-omics characterization reveals a distinctive metabolic signature and the role of NDUFA4L2 in promoting angiogenesis, chemoresistance, and mitochondrial dysfunction in clear cell renal cell carcinoma - PMC. https://pmc.ncbi.nlm.nih.gov/articles/PMC6326659/. Accessed 14 May 2025
27. Bianchi C, Meregalli C, Bombelli S, et al. The glucose and lipid metabolism reprogramming is grade-dependent in clear cell renal cell carcinoma primary cultures and is targetable to modulate cell viability and proliferation. Oncotarget. 2017;8:113502–15. https://doi.org/10.18632/oncotarget.23056.
28. Liu Z, Zhou Q, Wang Z, et al. Intratumoral TIGIT+ CD8+ T-cell infiltration determines poor prognosis and immune evasion in patients with muscle-invasive bladder cancer. J ImmunoTher Cancer. 2020;8: e000978. https://doi.org/10.1136/jitc-2020-000978.
29. Katayama N, Ohuchida K, Son K, et al. Tumor infiltration of inactive CD8 + T cells was associated with poor prognosis in gastric cancer. Gastric Cancer. 2025;28:211–27. https://doi.org/10.1007/s10120-024-01577-4.
30. Fix SM, Forget M-A, Sakellariou-Thompson D, et al. CRISPR-mediated TGFBR2 knockout renders human ovarian cancer tumor-infiltrating lymphocytes resistant to TGF-β signaling. J ImmunoTher Cancer. 2022;10: e003750. https://doi.org/10.1136/jitc-2021-003750.
31. Lasorsa F, Rutigliano M, Milella M, et al. Complement system and the kidney: its role in renal diseases, kidney transplantation and renal cell carcinoma. Int J Mol Sci. 2023;24:16515. https://doi.org/10.3390/ijms242216515.
32. Lucarelli G, Loizzo D, Franzin R, et al. Metabolomic insights into pathophysiological mechanisms and biomarker discovery in clear cell renal cell carcinoma. Expert Rev Mol Diagn. 2019;19(5):397–407. https://doi.org/10.1080/14737159.2019.1607729.
33. Sakaguchi S, Yamaguchi T, Nomura T, Ono M. Regulatory T cells and immune tolerance. Cell. 2008;133:775–87. https://doi.org/10.1016/j.cell.2008.05.009.
34. Mao X, Xu J, Wang W, et al. Crosstalk between cancer-associated fibroblasts and immune cells in the tumor microenvironment: new findings and future perspectives. Mol Cancer. 2021;20:131. https://doi.org/10.1186/s12943-021-01428-1.
35. The cross-talk between Abl2 tyrosine kinase and TGFβ1 signalling modulates the invasion of clear cell renal cell carcinoma cells - de marco - 2023 - FEBS letters - wiley online library. https://febs.onlinelibrary.wiley.com/. Accessed 14 May 2025. https://doi.org/10.1002/1873-3468.14531
36. Dudley AC. Tumor endothelial cells. Cold Spring Harb Perspect Med. 2012;2: a006536. https://doi.org/10.1101/cshperspect.a006536.
37. Ozel I, Duerig I, Domnich M, et al. The good, the bad, and the ugly: neutrophils, angiogenesis, and cancer. Cancers. 2022;14:536. https://doi.org/10.3390/cancers14030536.
38. Lu D, Li Y, Niu X, et al. STAT2/SLC27A3/PINK1-mediated mitophagy remodeling lipid metabolism contributes to pazopanib resistance in clear cell renal cell carcinoma. Research. 2024;7:539. https://doi.org/10.34133/research.0539.
39. Wang Z, Chen W, Zuo L, et al. The fibrillin-1/VEGFR2/STAT2 signaling axis promotes chemoresistance via modulating glycolysis and angiogenesis in ovarian cancer organoids and cells. Cancer Commun. 2022;42:245–65. https://doi.org/10.1002/cac2.12274.
40. Huo J, Wu L, Zang Y. Construction and validation of a universal applicable prognostic signature for gastric cancer based on seven immune-related gene correlated with tumor associated macrophages. Front Oncol. 2021;11: 635324. https://doi.org/10.3389/fonc.2021.635324.
41. Kuang S, Zhang J, Huang N, et al. The cumulative antitumor effects of regorafenib and radiotherapy in hepatocellular carcinoma. Mol Carcinog. 2024;63:1738–49. https://doi.org/10.1002/mc.23769.
42. Tolkach Y, Ellinger J, Kremer A, et al. Apelin and apelin receptor expression in renal cell carcinoma. Br J Cancer. 2019;120:633–9. https://doi.org/10.1038/s41416-019-0396-7.
43. Dogra S, Neelakantan D, Patel MM, et al. Adipokine apelin/APJ pathway promotes peritoneal dissemination of ovarian cancer cells by regulating lipid metabolism. Mol Cancer Res. 2021;19:1534–45. https://doi.org/10.1158/1541-7786.MCR-20-0991.
44. Master A, Wójcicka A, Piekiełko-Witkowska A. Untranslated regions of thyroid hormone receptor beta 1 mRNA are impaired in human clear cell renal cell carcinoma. Biochim Biophys Acta Mol Basis Dis. 2010;1802:995–1005. https://doi.org/10.1016/j.bbadis.2010.07.025.
45. Wojcicka A, Piekielko-Witkowska A, Kedzierska H, et al. Epigenetic regulation of thyroid hormone receptor beta in renal cancer. PLoS ONE. 2014;9: e97624. https://doi.org/10.1371/journal.pone.0097624.
46. Pearce EL, Poffenberger MC, Chang C-H, Jones RG. Fueling immunity: insights into metabolism and lymphocyte function. Science. 2013;342:1242454. https://doi.org/10.1126/science.1242454.
47. Yang J, Song X, Chen Y, et al. PLCγ1–PKCγ signaling-mediated Hsp90α plasma membrane translocation facilitates tumor metastasis. Traffic. 2014;15:861–78. https://doi.org/10.1111/tra.12179.
48. Sharma P, Allison JP. Immune checkpoint targeting in cancer therapy: towards combination strategies with curative potential. Cell. 2015;161:205–14. https://doi.org/10.1016/j.cell.2015.03.030.
49. Lasorsa F, Rutigliano M, Milella M, et al. Cellular and molecular players in the tumor microenvironment of renal cell carcinoma. J Clin Med. 2023;12:3888. https://doi.org/10.3390/jcm12123888.
50. Shahvali S, Rahiman N, Jaafari MR, Arabi L. Targeting fibroblast activation protein (FAP): advances in CAR-T cell, antibody, and vaccine in cancer immunotherapy. Drug Deliv Transl Res. 2023;13:2041–56. https://doi.org/10.1007/s13346-023-01308-9.
51. Lucarelli G, Netti GS, Rutigliano M, et al. MUC1 expression affects the immunoflogosis in renal cell carcinoma microenvironment through complement system activation and immune infiltrate modulation. Int J Mol Sci. 2023;24:4814. https://doi.org/10.3390/ijms24054814.
52. Vuong L, Kotecha RR, Voss MH, Hakimi AA. Tumor microenvironment dynamics in clear cell renal cell carcinoma. Cancer Discov. 2019;9:1349–57. https://doi.org/10.1158/2159-8290.CD-19-0499.
53. Netti GS, Lucarelli G, Spadaccino F, et al. PTX3 modulates the immunoflogosis in tumor microenvironment and is a prognostic factor for patients with clear cell renal cell carcinoma. Aging. 2020;12:7585–602. https://doi.org/10.18632/aging.103169.
54. Lucarelli G, Rutigliano M, Loizzo D, et al. MUC1 tissue expression and its soluble form CA15-3 identify a clear cell renal cell carcinoma with distinct metabolic profile and poor clinical outcome. Int J Mol Sci. 2022;23:13968. https://doi.org/10.3390/ijms232213968.
55. Milella M, Rutigliano M, Lasorsa F, et al. The role of MUC1 in renal cell carcinoma. Biomolecules. 2024;14:315. https://doi.org/10.3390/biom14030315.

56. Tamma R, Rutigliano M, Lucarelli G, et al. Microvascular density, macrophages, and mast cells in human clear cell renal carcinoma with and without bevacizumab treatment. Urol Oncol Semin Orig Investig. 2019;37:355.e11-355.e19. https://doi.org/10.1016/j.urolonc.2019.01.025.
57. Metabolomics to assess response to immune checkpoint inhibitors in patients with non-small-cell lung cancer - PMC. https://pmc.ncbi.nlm.nih.gov/articles/PMC7760033/. Accessed 14 May 2025
58. Salem ME, Bodor JN, Puccini A, et al. Relationship between MLH1, PMS2, MSH2 and MSH6 gene-specific alterations and tumor mutational burden in 1057 microsatellite instability-high solid tumors. Int J Cancer. 2020;147:2948–56. https://doi.org/10.1002/ijc.33115.
59. Patergnani S, Danese A, Bouhamida E, et al. Various aspects of calcium signaling in the regulation of apoptosis, autophagy, cell proliferation, and cancer. Int J Mol Sci. 2020;21:8323. https://doi.org/10.3390/ijms21218323.
60. Ashton TM, McKenna WG, Kunz-Schughart LA, Higgins GS. Oxidative phosphorylation as an emerging target in cancer therapy. Clin Cancer Res. 2018;24:2482–90. https://doi.org/10.1158/1078-0432.CCR-17-3070.
61. Monteith GR, Davis FM, Roberts-Thomson SJ. Calcium channels and pumps in cancer: changes and consequences. J Biol Chem. 2012;287:31666–73. https://doi.org/10.1074/jbc.R112.343061.
62. Weinberg SE, Chandel NS. Targeting mitochondria metabolism for cancer therapy. Nat Chem Biol. 2015;11:9–15. https://doi.org/10.1038/nchembio.1712.
63. Maher RL, Branagan AM, Morrical SW. Coordination of DNA replication and recombination activities in the maintenance of genome stability. J Cell Biochem. 2011;112:2672–82. https://doi.org/10.1002/jcb.23211.
64. Strickler JH, Hanks BA, Khasraw M. Tumor mutational burden as a predictor of immunotherapy response: Is more always better? Clin Cancer Res. 2021;27:1236–41. https://doi.org/10.1158/1078-0432.CCR-20-3054.
65. Tong W, Wang G, Zhu L, et al. Pan-cancer analysis identified CD93 as a valuable biomarker for predicting patient prognosis and immunotherapy response. Front Mol Biosci. 2022;8: 793445. https://doi.org/10.3389/fmolb.2021.793445.